ACS APPLIED NANO MATERIALS

www.acsanm.org Article

# Functionalized Ag Nanoparticles Embedded in Polymer Resists for High-Resolution Lithography

Mohamad G. Moinuddin, Rudra Kumar, Midathala Yogesh, Shivani Sharma, Manoj Sahani, Satinder K. Sharma,* and Kenneth E. Gonsalves*

Cite This: https://dx.doi.org/10.1021/acsanm.0c01362 Read Online

ACCESS | Metrics & More | Article Recommendations | Supporting Information

**ABSTRACT:** Extending the resolution limit of next-generation lithography down to 15 nm or below requires the resist to attain small features, high irradiation sensitivity, and low line edge/width roughness. To meet this prerequisite, an increase of irradiation absorption in resists is an important strategy. A negative tone, deep ultraviolet, electron beam, and helium ion beam active resist formulation has been realized comprising a hydroxystyrene-based polymer *tert*-butyl 2-ethyl-6-(4-hydroxyphenyl)-4-phenylheptanoate (Terpolymer). Further, the resist performance was enhanced by doping of a microemulsion-based Ag nanoparticle (size distribution ∼2 nm) irradiation sensitizer. As a result, a tenfold decrease in the critical dose ($E_o$) was observed by increasing Ag nanoparticle contents from 0.1 to 1.0 wt %. The developed resist patterns exhibit significantly higher sensitivities and resolutions of 50 and 34.12 $\mu$C/cm$^2$ and ∼12 and ∼11 nm line patterns, respectively, for e-beam ($E_e$) and helium ion beam ($E_{He}$) irradiations. The line edge/width roughness of well-developed e-beam exposed patterns was found to be 1.5 ± 0.1/2.8 ± 0.3 nm, respectively. These e-beam/resist interactions were modeled by the Monte-Carlo trajectory, and the results were in line with the experimentally observed one. These simulations suggest the enhanced irradiation absorption inside the resist matrix with the addition of a high-electron-density Ag entity. These investigations reveal that one of the best ways to simultaneously improve the sensitivity and resolution of the resist is the optimum incorporation of higher-atomic-number nanoparticles in the polymeric matrix, which enhances the absorption cross section ($\sigma$) without altering the resist properties.

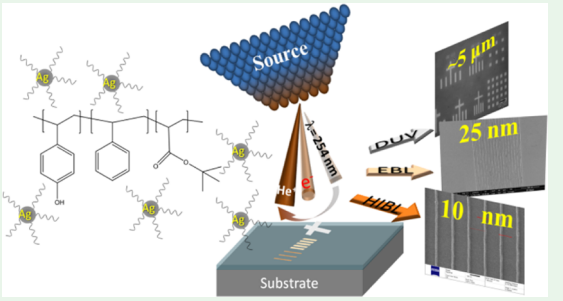


**KEYWORDS:** *next-generation lithography, negative tone resist, functionalized Ag nanoparticles, irradiation sensitizer, Monte-Carlo e-beam trajectory simulation*



## 1. INTRODUCTION

The miniaturization of electronic devices has mainly been stimulated by the progress of lithography technologies and advancement in innovative resist compositions.[1] The novel patterning technologies are experiencing the fast development of various next-generation lithography tools to meet the ever-increasing market demand for high-performance electronic devices.[2−9] The leading irradiation-based lithography technologies including electron beam lithography (EBL), extreme-ultraviolet lithography (EUVL), and helium ion beam lithography (HIBL) have already proven their potential in photoresist patterning down to single-digit resolution.[10−12] Among these, electron beam lithography (EBL) has widely been adapted for high-resolution lab-scale device processing and prototyping down to sub-15 nm features. However, the major hurdle with EBL is its slow processing speed, especially at the time of writing dense patterns over a large area, and this could be the sole reason for its not being considered as a tool for high-volume manufacturing. Recently, multibeam irradiations have been explored in EBL to increase the patterning speed.[13] Apart from EBL, helium ion beam lithography (HIBL) possesses a higher-energy $He^+$ ion beam with significantly less scattered paths inside the resist, contrary to EBL electrons. High-energy $He^+$ ions result in better resolution and sensitivity along with negligible proximity effect.[14−16] Moreover, as HIBL is capable of patterning features with a very small size, it can serve as a stringent test to the performance potential of resists.[17] Another major aspect of high-resolution lithography is the resist material used for patterning. The less availability of compatible resists having high resolution ($R$), low line edge/width roughness ($L$), and high sensitivity ($S$) requires new resist formulations to handle the RLS tradeoff.[18] The major bottleneck faced while developing resists is the poor sensitivity ($E_o$) toward irradiation, leading to high dose requirements.[19] Therefore, the improvement in resist sensi-

Received: May 19, 2020
Accepted: August 4, 2020
Published: August 4, 2020

tivity can be achieved through material engineering or through developing innovative physiochemical technology for these materials.

As far as resists are concerned, chemically amplified resists (CARs) have been wildly used in the semiconductor industries in the past decades due to their good sensitivity ($E_o$). Their $E_o$ depends on the nature of the photoacid generator (PAG) and its concentration inside the resist formulation.[20] In this progress, Nandi et al. has produced high-aspect-ratio patterns of 100 nm with an ionic photoacid generator-included Terpolymer photoresist, viz., GBLMA−MAMA−MAPDST.[21] Apart from CARs, hybrid resists are also being considered as emerging candidates for current lithography technology mainly due to their patterning potential for high-resolution features in the absence of PAGs in resist compositions.[22−25] Similarly, metal−organic clusters and methacrylate-based materials without any PAG have also been reported with notable sensitivity toward all types of irradiations.[26−30] Recently, our group developed nickel-based negative tone resists using EBL/HIBL and showed sub-10 nm line patterning.[30,31] Also, the negative tone chromium-containing resists revealed the patterning capability and high-etch resistance to silicon and tungsten at sub-10 nm resolution.[16]

In continuation of this, the patterning feature sizes are also governed by resist thickness. Recently, Lewis et al. reported the formation of 7 nm negative tone patterns with only ∼4 nm thick film.[16] However, the decrease in film thickness reduces the absorption cross section of the irradiation, resulting in poor patterning yield.[32,33] Furthermore, in the case of high-energy irradiation, most of the resist thin films are almost transparent. Average of ∼20% irradiation can be absorbed by these films depending upon the sensitivity of resist formulation and volume over the substrate.[34] Hence, the sensitivity of the resist can be improved through the incorporation of a high irradiation absorber entity in the resist formulation.[35] In this regard, insertion of high-atomic-number nanomaterials in the resist formulation plays a significant role in high-speed lithography applications.[22,36] Also, the irradiation absorption cross sections ($\sigma$) of metal nanoparticles (such as Au, Ag, and Sn) are considerably greater than that of carbon or oxygen in resists, which eventually enhances the resist sensitivity.[37,38] Thus, the amalgamation of high-atomic-number metal nanoparticles in the polymer matrix may lead to the development of resists with better mechanical and chemical properties, high sensitivity, low line edge roughness/line width roughness (LER/LWR), and low CD through the enhanced absorption of exposure radiation.[26,23] Silver nanostructures that have been embedded in the polymer matrix were reported widely in the literature.[39,40] In this regard, silver nanoparticles were embedded in the SU8 photoresist that creates a conductive photoresist with various structures.[41] Recently, the silver salt solution was mixed with the S1805 Novolac-based positive tone photoresist and exposed in EBL to develop features of 10 $\mu$m.[42] Apart from silver nanoparticles, patterning of silver nanowire films was demonstrated for the application in organic light-emitting diodes.[43,44]

Herein, we report a new resist formulation strategy to answer the advanced lithography application using a high-speed patterning approach and high-absorption resist materials. We have successfully developed an effective resist composition of ultrafine silver nanoparticles (Ag-NPs) embedded in the *tert*-butyl 2-ethyl-6-(4-hydroxyphenyl)-4-phenylheptanoate (Terpolymer) polymeric matrix. First, we demonstrated Terpolymer as a free-standing negative tone resist material. After that, microemulsion-based Ag-NPs and Terpolymer were blended with varied feed ratios to understand the effect of Ag-NPs on hybrid resist formulation. Moreover, the resist formulations with different feed ratios of Ag-NPs embedded in Terpolymer were found to be sensitive to a broad range of irradiations such as deep ultraviolet (DUVL), EBL, and HIBL with good resist sensitivity. The Monte-Carlo simulation suggested that the incorporation of Ag-NPs densifies the resist film and increases the $\sigma$ many folds. The systematic studies demonstrated that the embedded Ag-NPs in the resist may tune the sensitivity as well as the characteristics of otherwise known resist materials.

## 2. EXPERIMENTAL SECTION

**2.1. Materials.** Silver nitrate ($AgNO_3$), dioctyl sulfosuccinate sodium salt (AOT), toluene, and hydrazine hydrate ($N_2H_4H_2O$) were purchased from Sigma-Aldrich. All of the chemicals were used as received without any further purification. Deionized water with 18.2 MΩ·cm was produced using the Millipore DI water plant.

**2.2. Synthesis of the Resist.** *2.2.1. Synthesis of the Terpolymer Resist.* Hydroxystyrene-based Terpolymer (chemical structure in Figure 1a) was synthesized using the free radical polymerization

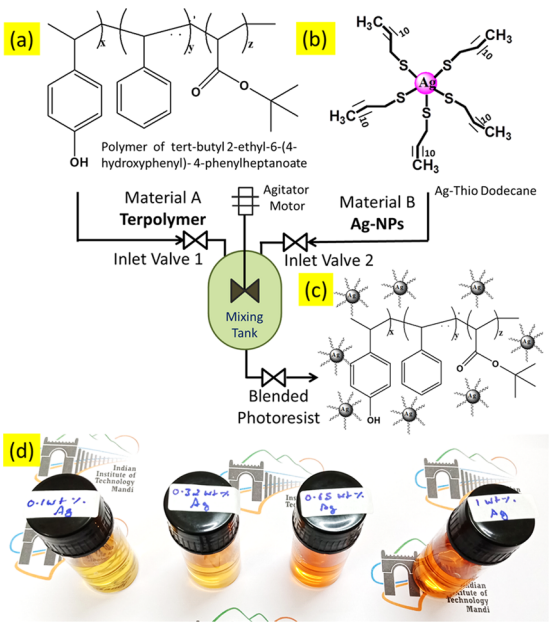


**Figure 1.** Chemical structure of (a) *tert*-butyl 2-ethyl-6-(4-hydroxyphenyl)-4-phenylheptanoate polymer (Terpolymer) resist, (b) Ag-thio-dodecane (Ag-NP) and (c) blended Ter−Ag. (d) Color contrast of blended solutions.

procedure as given in the literature (detailed synthesis is mentioned in SI-1 (Figure S1)).[45] The pristine Terpolymer (abbreviated as Ter) and Terpolymer with iodonium PAG (the PAG was fixed to 3 wt % w.r.t. to Terpolymer; PAG description available in Figure S2), denoted reference (Ter-PAG), were well dissolved in ethyl lactate.[46]

*2.2.2. Synthesis of Ag Nanoparticles (Ag-NPs).* Ultrafine silver nanoparticles (Ag-NPs) were prepared by the water-in-oil (W/O) microemulsion technique. Briefly, 0.05 M AOT was added dropwise to 2 mL of 0.005−0.02 M silver nitrate with continuous stirring at 600 rpm for 5 min until the solution becomes milky. After that 8 mL of toluene was added into the solution and stirred for another 10 min. Subsequently, 0.2 mL of hydrazine hydrate was added dropwise and the resulting solution was kept for 1 h with continuous stirring. After completion of the reaction, the well-dispersed silver nanoparticles were collected by centrifugation and washed with ethanol and water.


https://dx.doi.org/10.1021/acsanm.0c01362
ACS Appl. Nano Mater. XXXX, XXX, XXX−XXX

In the postprocessing step, the washed Ag-NPs were collected in toluene and caped with organic ligands (thio-dodecane) to avoid agglomeration. Figure S3 shows the process flow for preparing well-dispersed functionalized ultrafine Ag-NP formulations, and the final expected chemical structure of synthesized Ag-NP is shown in Figure 1b.

*2.2.3. Blending of Well-Dispersed Ag-NP with Terpolymer.* The ultrafine Ag-NPs were blended with synthesized Terpolymer in different ratios of 3:97, 6:94, 12:88, and 36:64 (% vol/vol) in an ethyl lactate solution at room temperature under a nitrogen atmosphere. Briefly, Ag-NPs dispersed in toluene were slowly transferred through the phase-transfer reaction to the ethyl lactate solution containing the Terpolymer with continuous stirring at room temperature for 4−6 h, as shown in Figure S3. After this step, the solvent was evaporated through a vacuum rotary evaporator, and the solid residue obtained was collected. Figure 1c depicts the possible chemical structure of the synthesized blend. Final Ag-NP-embedded Terpolymer (acronym Ter−Ag will be used) solutions with a different set of feed ratios have been formulated and are depicted in Figure 1d. Furthermore, to analyze the actual wt % of Ag-NPs embedded inside Terpolymer, a calculation for wt % of Ag-NPs within the per unit volume of toluene was adapted. It was considered that the amount of Ag salt taken in the initial stage was transformed in well-dispersed ultrafine Ag-NP synthesis. The analyzed wt % values of ultrafine Ag-NPs in Ter−Ag formulation are 3 → 0.1, 6 → 0.3, 12 → 0.65, and 36 → 1.01 (vol % → wt %).

**2.3. Thin Film Preparation.** The pristine (Terpolymer), reference (Ter-PAG), and Ag-NP hybrid (Ter−Ag) resist solutions were prepared in ethyl lactate with the aid of the vortex mixture; the wt % values in ethyl lactate were kept constant to 2 wt % (20 mg/mL resist) for all samples. Then, the solution was filtered through a 0.22 $\mu$m Teflon membrane via a syringe filter to remove the unwanted bigger particles. After that, the solution was spin-coated at different speeds (3000−4500 rpm) for 45 s on RCA-cleaned silicon wafers to form ∼40 nm thin films. Thin-film-coated wafers were prebaked at 70 °C for 60 s to remove the excess solvent. In general, metal-bearing solutions face issues in uniform film formation and it introduces the contamination to the semiconductor processing also.[23] Figure S4a shows the optical micrograph of the uniform coating of Ter−Ag, which could be due to the capping of Ag-NPs with organic moieties. Figure S4b was produced from the scratched Ter−Ag resist thin film (used for thickness measurement) and mesured thickness was 44 ± 2 nm.

**2.4. Lithography.** The prebaked thin film wafers were exposed to deep ultraviolet (DUV; $\lambda$ ∼ 254 nm) with a power of ∼1.5 mW/cm$^2$ for 2 min. After the exposure, the thin films were baked at 60 °C for 60 s. The pattern development process was optimized with different developers such as tetramethylammonium hydroxide (TMAH), tetrabutylammonium hydroxide (TBAH), and acetonitrile (ACN) followed by a rinse with DI water. Further, high-resolution patterns were realized using electron beam lithography (EBL) (e-Line Plus, Raith GmbH). EBL patterning was performed by the exposure of 20 keV energy with various energy doses; during the EBL process, the beam current was kept constant at 22.3 pA; the extended procedure is mentioned elsewhere.[30] Finally, high-resolution/high-speed patterning was established with the advanced helium ion beam lithography (HIBL) (Zeiss ORION Nano-Fab system) technique. For HIBL patterning, a beam current of ∼1.0 pA from a 10 $\mu$m numerical aperture were used. After the exposure, samples were developed using a recipe standardized during DUVL.

**2.5. Characterization.** The surface morphology of synthesized ultrafine silver nanoparticles was characterized by transmission electron microscopy (TEM, Tecnai G2 20 S-TWIN, FEI). Scanning electron microscope (FESEM, Zeiss, Zemini 500, Germany) was used to analyze the patterned resist. The particle size was measured by the dynamic light scattering (Zetasizer Nano-ZS, Malvern Panalytical) method. Surface characteristics of thin films and patterned resist films were analyzed by an optical microscope (Olympus 251BX). Thin patterned resist films were also characterized by atomic force microscopy (AFM, Bruker, Dimension Icon, Germany). The molecular weight of the polymer was determined by gel permeation chromatography (GPC, Agilent Technology, model no. 1260).

**2.6. Electron Beam Trajectory Simulation.** The effect of ultrafine Ag-NPs on the e-beam trajectory inside the resist films has been analyzed using the Monte-Carlo (MC) simulation tool CASINO, v2.5.1.0.[47] MC simulations are wildly used for e-beam and matter interaction approximation. Many electrons of fixed beam energy (20 keV used) are programmed to strike the target (resist/substrate heterostructure). These interactions further decide the intensities of backscattered and secondary electron signals that mostly depend upon the target material density, absorption coefficient ($\sigma$), and conductivity. These intensities applied to develop metrology of thin film/substrate interactions in EBL. The literature suggests that these MC simulations provide an almost similar trajectory to that observed experimentally.[48] Herein, the trajectory analysis was performed with the density of the resist using the monomer configuration of Terpolymer ($C_{25}H_{34}O_3$), and further, Ag-NPs ($AgS_5C_{60}H_{125}$) were added to analyze the effect. The e-beam spot was fixed to 0.5 nm, and the number of trajectories was kept constant to 5600.[49]

## 3. RESULTS AND DISCUSSION

The transmission electron microscopy (TEM) micrographs of microemulsion-based synthesized ultrafine Ag-NPs are shown in Figure 2a. A monodispersed and uniform size distribution of

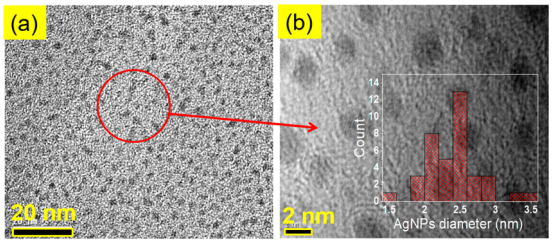


**Figure 2.** (a) Uniform distribution of bare ∼2 nm Ag-NPs coated on the copper TEM grid. (b) Zoomed area shows a uniform and crystalline Ag core; the histogram is produced by analyzing the same image.

∼2 nm clearly showed the successful formation of ultrafine Ag-NPs by the phase-separated microemulsion synthesis technique. Further, the average particle size of ultrafine Ag-NPs was ∼2 nm, as verified by the dynamic light scattering method, as shown in Figure S5, and supported by the TEM analysis, as depicted in Figure 2b. The average molecular weight of Terpolymer was determined to be ∼12 600 kg/mol with a polydispersity index of 1.7 by the gel permeation chromatography (GPC) method, as depicted in Figure S6.

**3.1. Analysis of Terpolymer Resist Patterning.** The synthesized pristine Terpolymer and ultrafine Ter−Ag hybrid resists were spin-coated on RCA-cleaned silicon wafers (2 × 2 cm$^2$) to check the thin film formation. Sets of reference Ter-PAG samples were also coated in the same manner for DUVL and EBL investigation, as mentioned in Section 2.3. First, pristine Terpolymer was realized as a negative tone resist in contrast with the conventional Ter-PAG (Figure S7b). Ter-PAG showed a positive tone pattern in TMAH (0.26 N), as featured in Figures 3a and S7a, whereas the pristine Terpolymer resulted in the negative tone poor patterns, as shown in Figure S7b.[50] Second, the synthesized Ter−Ag resist was exposed under DUVL with a threshold sensitivity ($E_o$) of 150 mJ/cm$^2$. At the outset, these Ter−Ag films were developed in TMAH and showed broken patterns like pristine Terpolymer, which may be due to fast dissolution in the


https://dx.doi.org/10.1021/acsanm.0c01362
ACS Appl. Nano Mater. XXXX, XXX, XXX−XXX

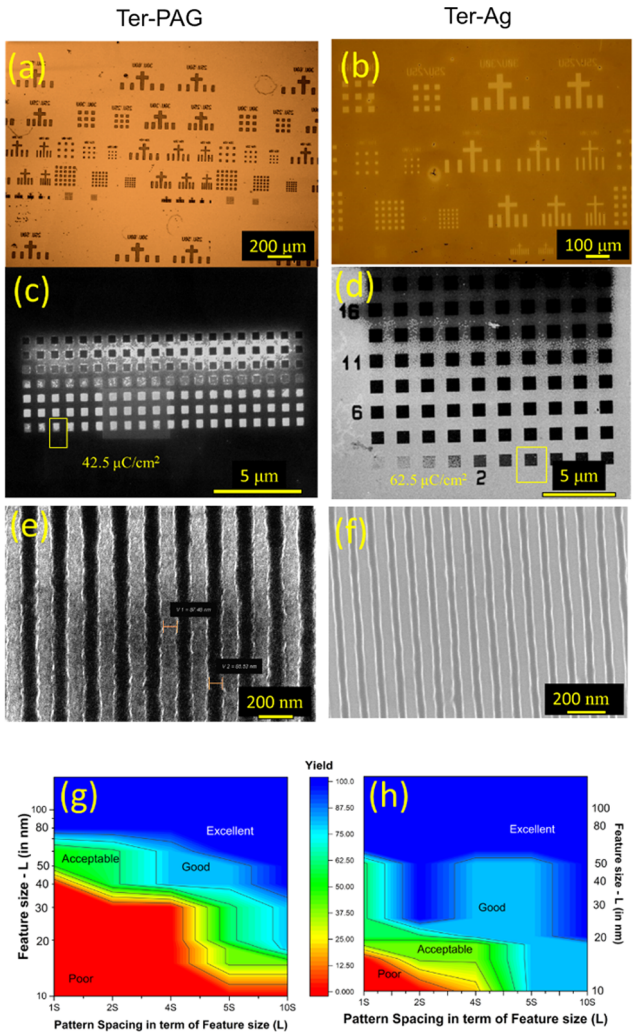


**Figure 3.** Realization of Terpolymer as a negative tone resist and its comparison with conventional positive tone Ter-PAG. The DUV-exposed pattern on the Terpolymer resist with (a) Ter-PAG (3 wt %) and (b) Ter–Ag (1 wt %). e-Beam sensitivity analysis of (c) Ter-PAG and (d) Ter–Ag, suggesting an almost similar sensitivity of ∼40–75 $\mu C/cm^2$. High-resolution SEM image of half-pitch patterns in (e) Ter-PAG (85 nm) and (f) Ter–Ag (50 nm). Investigation into the patterning yield approximation for 20 keV e-beam exposure in (g) Ter-PAG and (h) Ter–Ag.

basic developer. Further, mild polarity developers (w.r.t. TMAH) were adapted for pattern generation using TBAH and acetonitrile (ACN), as shown in Figure S8a–c. Well-developed negative tone patterns are formed in ACN, and their optical images are presented in Figure 3b. A larger preview of the optical micrograph is shown in Figure S8d, which demonstrates the sharp patterns with various shapes and sizes (minimum features showed as ∼5 $\mu$m).

After the successful exposure and development in DUV patterns, a further in-depth examination through the comparative study of the electron-beam-exposed Terpolymer resist formulation was performed. Terpolymer was examined in EBL with two blendings (1) reference PAG and (2) newly synthesized Ag-NPs, and the outcomes are shown in Figure 3c–h. The variable dose exposure (base dose was fixed to 25 $\mu C/cm^2$ with an increment step of 7.5 $\mu C/cm^2$) was performed for both Ter-PAG and Ter–Ag resist formulations. Figure 3c shows the positive tone SEM micrograph of the Ter-PAG pattern with the critical dose ($E_e$) of 42.5 $\mu C/cm^2$. These patterning results corresponded to 3 wt % PAG w.r.t. Terpolymer, and the amount of the critical PAG concentration was selected due to the heavy thickness loss during the development process when used a lesser amount of PAG. The high-resolution exposure provides well-developed patterns of 80 nm, as shown in Figure 3e. These patterns depict high edge roughness, which suggests the limitation of Terpolymer when blended with the PAG.[21] On the other hand, when Ag-NPs were blended with Terpolymer, the resist formulation provides negative tone patterns, as shown in Figure 3d. The critical sensitivity ($E_e$) for 1 wt % Ter–Ag was found to be 50–62.5 $\mu C/cm^2$, which is in line with the reference Ter-PAG resist. Figure 3f shows the neat pattern of 50 nm L/S with extremely decreased edge roughness and a prelude to smaller-dimension pattern generation.

The comparative study between newly developed Ter–Ag and Ter-PAG resist was performed under EBL to illustrate the patterning yield at different dimensions ranging from 10 to 150 nm and different line spacings from $L/S$ to $L/10S$. Figure 3g,h shows the patterning yield contour plot for all of the possible dimensions with various line spacings for both resists. Dark blue color depicts the corresponding feature size that can be easily patterned with high yield, and the red color describes the patterns that are unlikely to form. These contour plots corroborate the better yield and resolution when Terpolymer was realized as a negative tone resist in the presence of Ag-NPs (Figure 3h).

### 3.2. Effect of Ag-NPs on Ter–Ag Resist Performance.

The insertion of ultrafine Ag-NPs and its various effects have been studied on the hybrid resist formulations such as the modulation of NP concentration (wt %) and particle size (nm). The investigations suggested that a significant contribution of Ag-NPs in the lithography pattern generation is described as follows.

*3.2.1. Effect of Ultrafine Ag-NP Concentration.* The blending of ultrafine Ag-NPs into the Terpolymer matrix was varied from 0.1 to 1.0 wt %. It was observed that the sensitivity changed drastically from 600 to 50 $\mu C/cm^2$ when the Ag-NP loading was increased from 0.1 to 1.0 wt %. FESEM and AFM micrographs of e-beam-exposed Ter–Ag resist patterns w.r.t. the remaining thickness are shown in Figure S9. Figure 4a shows the sensitivity contrast curve of Ter–Ag for different loadings calculated with help of AFM data. It confirms the impact of the Ag-NP presence on sensitivity ($E_e$) of Terpolymer resist formulations. A relation between the normalized remaining thickness (NRT) and e-beam exposure dose in Figure 4a indicates that the remaining thickness of all Ter–Ag resist formulations increases with an increase in e-beam exposure dose, confirming a negative tone nature. The contrast ($\gamma$) and sensitivity ($E_e$) of 1 wt % Ag-NPs loaded in Ter–Ag were found to be ∼1.32 and ∼50.0 $\mu C/cm^2$, respectively. However, the $\gamma$ and $E_e$ of 0.1 wt % Ag-NPs loaded in Ter–Ag were found to be ∼1.35 and ∼600 $\mu C/cm^2$, respectively. However, it was depicted that the contrast ($\gamma$) of the resist had not been altered with an increase in loading of Ag-NPs (wt %) in the resist material, which suggests no attenuation of the polymer cross-linking property. All of the results obtained from this systematic study on Ag-NPs' impact on resist formulation confirmed that Ag-NPs can act as efficient irradiation sensitizers, making the resist more sensitive toward e-beam, which could also be the case for other high-resolution lithography exposure tools.


https://dx.doi.org/10.1021/acsanm.0c01362
ACS Appl. Nano Mater. XXXX, XXX, XXX–XXX

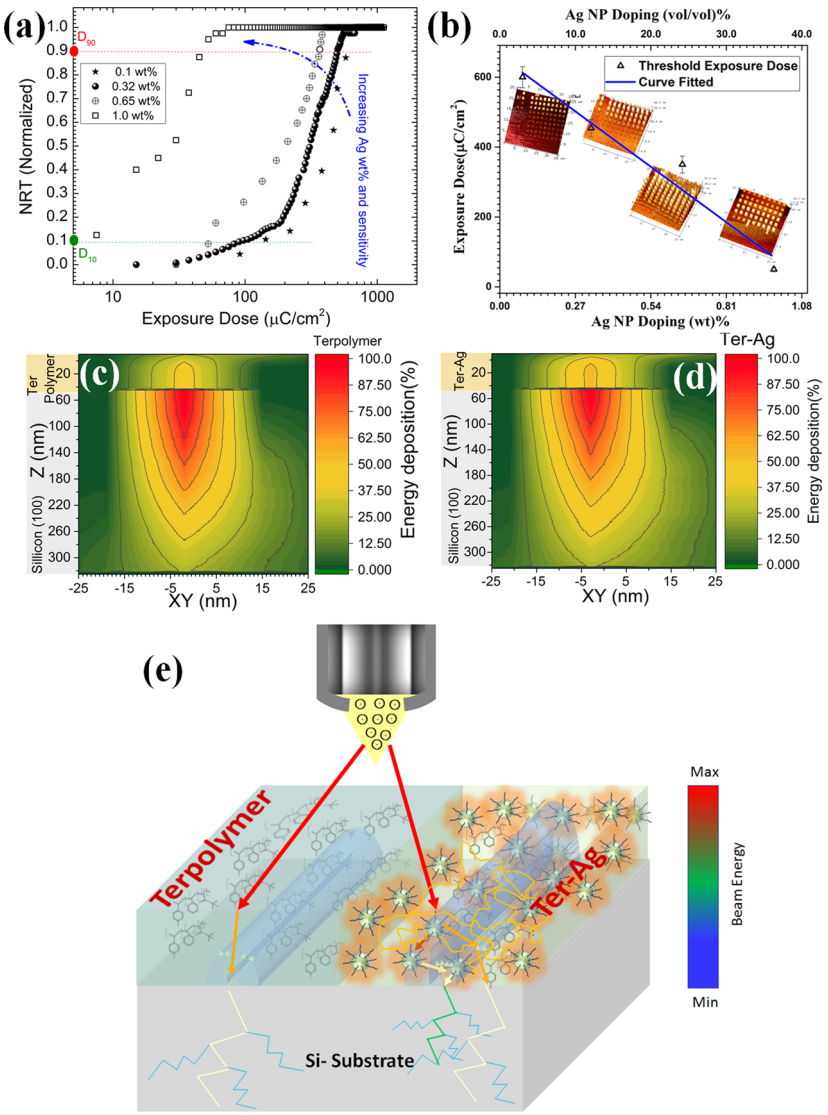


**Figure 4.** Effect of Ag-NP doping in resist formulation. (a) Sensitivity contrast curve and (b) effect of Ag-NPs over e-beam exposure dose. Energy distribution inside (c) pristine Terpolymer and (d) Ter−Ag; the 40 nm resist film was simulated in CASINO v.2.5.1.0 for 0.5 nm beam spot; the color bar depicts the fraction of energy/dose dispersed in the resist/Si system. (e) Typical irradiation exposure interaction mechanisms within the pristine Terpolymer formulation and ultrafine silver nanoparticles (Ag-NPs) incorporation in Ter−Ag formulation for high-resolution lithography patterning.

The $E_e$ vs Ag-NPs' wt % ($\phi$) was analyzed and fitted linearly with the assumption that the absorbed energy by Ag-NPs has been scattered or transferred to the nearby polymeric environment. It directly changes the physicochemical properties of the Terpolymer matrix, as shown in Figure 4b. It is interesting to note that the exposure dose was significantly decreased with increased loading of Ag-NPs possibly due to the increased absorbance of a large fraction of e-beam energy. At the same time, the better interpretation of high-resolution patterning performance as a result of Ag-NPs loading in Terpolymer and probable e-beam irradiation energy interaction within the polymeric matrix can be expressed mathematically.[46]

The actual absorption sensitivity ($E_{ab}$) of resist can be expressed by the following relation

$$E_{ab} = \sigma \times E_o \text{ and } E_o = \frac{\int i dt}{A} \text{ or } E_o = \frac{E_{ab}}{\sigma} \quad (1)$$

where $\sigma$, $E_o$, $i$, $A$, and d$t$ are the absorption cross section of the resist, incident dose/energy, beam current, area exposed under single irradiation, and the fraction of time, respectively. In the present study, exposure beam current ($i$) was kept constant with the concerned e-beam exposure tool, so eq 1 can be simplified as

$$E_{ab} = \sigma \frac{i \cdot \tau}{A}$$

where $\tau$ is the beam dwell time inside the resist.

The required minimum energy for physiochemical change ($E_{ab}$) in resist formulation would be nearly constant for unit volume (constant $A$). Therefore, a change in the absorption cross section ($\sigma$) will directly lead to a change in $\tau$

$$E_o \propto \tau \propto \frac{1}{\sigma} \quad (2)$$

Thus, an increase in the incorporation of absorption cross-section element in resist formulations leads to enhanced


https://dx.doi.org/10.1021/acsanm.0c01362
ACS Appl. Nano Mater. XXXX, XXX, XXX−XXX

sensitivity; a similar trend was observed in Figure 4b with a linear decay in the required dose for an increased fraction of Ag-NP loading in the resist matrix, as described in eq 2.

Based on the above investigations, a further systematic investigation into the resist absorbance effect is imperative. In this context, it is found that Terpolymer thin films possess low density (~0.78 g/cm$^3$; calculated for monomer Terpolymer in Casino v.2.5.1.0) due to the presence of low-atomic-number atoms, i.e., C, O, and H. Therefore, these resist films may found to be ~80% transparent to the high-energy irradiation such as EBL and HIBL.[51] However, the inclusion of high-atomic-number metal nanoparticles in the resist formulation densifies the films and also scatter the incident radiations to a large extent.[23] Similar behavior in the Ter−Ag matrix suggests the increased e-beam radiation scattering and enhanced absorption due to a higher $\sigma$ of Ag-NPs, as seen from the possible radiation interaction mechanism in Figure 4e. In the view of facts that the high-energy e-beam irradiations to pristine resist thin film result in fewer effective collisions and require high exposure dose. On the other hand, increased collisions inside the Ter−Ag will enhance sensitivity, majorly due to two types of successive scattering: elastic (energy is conserved and beam scatters laterally) and inelastic (energy is transferred to the target material). To support the elastic and inelastic energy electron-resist scattering interaction mechanism of the present work, a conceptual understanding of the numerical model reported by Henderson et al., is used (see SI-13).[35] In elastic collision, electron−atom interaction can be explained by Rutherford scattering cross sections ($\sigma_{el}$) as $\sigma_{el} \propto Z_i$, where $Z_i$ corresponds to the atomic number,[52] while in the case of inelastic collision, the incident beams ionize the atom core/valance band and generate free electrons (called secondary electrons). If secondary electrons possess enough energy such as >50 eV, it initiates further physiochemical change inside the resist atoms.[53]

To understand the corresponding qualitative behaviors, the basic Monte-Carlo trajectory analyses were simulated and depicted in Figure S10. For the resist/substrate hetero-structure, Monte-Carlo simulations of resist (40 nm)/silicon were realized by considering the chemical structure, as shown in Figure 1a,b. Figure 4c shows the simulated depth trajectory ($X$−$Z$) for 20 keV e-beam irradiations (beam spot 0.5 nm). The color bar depicts the fraction of energy distributed (in %) within the resist film and substrate. The energy distribution of e-beam suggests that 20−25% absorption in pristine Terpolymer might be due to low density. To decrease the transmittance of the resist film under e-beam irradiation, the Ag-NP chemical entity was added to the resist molecular formula, and the resulted trajectory is depicted in Figure 4d. It was also observed that the loading of Ag-NPs in the Terpolymer matrix resulted in resist film densification. Figure 4d indicates that there is an increase in energy distribution inside the resist film from 25% (Figure 4c) to ~50%. So, for the same Terpolymer resist, the incident exposure dose ($E_o$) should be decreased by a factor $\sigma$, as mentioned above.

*3.2.2. Effect of Ag-NP Size on Pattern Morphology.* As discussed in previous sections, the concentration of Ag-NPs plays an important role in enhancing the resist sensitivity. Alternatively, the size and morphological distribution of ultrafine Ag-NPs also play a key role. It is important to notice that the nanoparticles mainly act as sensitizers, and other than this, there is no direct contribution of the resist to the physicochemical change. Figure 5 shows the effect of Ag-NPs

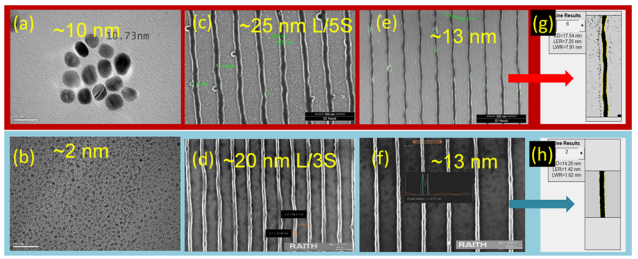


**Figure 5.** Effect of Ag-NP size on nanopatterning. TEM image of Ag nanoparticles with even size distributions of (a) ~10 nm and (b) ~2 nm; the large size nanoparticles affect the pattern morphology (c, e), whereas homogeneous ~2 nm particles have less effect as shown in (d, f); and computed edge roughness for isolated 13 nm patterns corresponding to the size distribution of ~10 nm (g) and ~2 nm (h).

size on resist patterning and morphological distribution of EBL-exposed patterns. Figure 5a depicts the TEM micrograph of ultrafine Ag nanoparticles in toluene and corresponds to 0.02 M metal salt; these Ag-NPs are loaded in Terpolymer to form Ter−Ag 1 wt %. However, some buckling in the line patterns of Ter−Ag (25 and 13 nm features) is visible possibly due to the incorporation of large (~10 nm) Ag-NPs, as shown in Figure 5c,e. Also, these investigations reveal that substantial pattern buckling occurs when the pattern resolutions are in the range of the dimension of NPs. This apparent influence of Ag-NPs on the patterning potential of hybrid resists possibly elucidates that there is no postexposure change in the Ag-NP chemistry.[54]

Further, Figure 5b shows the ~2 nm ultrafine Ag-NPs (correspond to 0.005 M metal solt) which were loaded in Terpolymer to form 1 wt % Ter−Ag blend. Figure 5d,f depicts the defect-free patterns as compared to the ~2 nm NPs incorporation in Ter−Ag patterns. The computed line edge/line width roughness (LER/LWR) analyses reveal a fivefold improvement in reducing roughness from 7.2 to 1.6 nm with a reduction of NP size from ~10 to ~2 nm. For the average 13 nm line feature sizes, the measured LERs for various sizes of Ag-NPs loading are found to be 17.5 ± 7.2 and 14.2 ± 1.4 nm, respectively, as shown in Figure 5g,h (the calculation of LER/LWR is explained in Figures S11−S13). It evidentially indicates that the dimension and distribution of nanoparticles play a vital role in the formation of high-resolution well-developed patterns and hence affect the device structure as output. Considering these results and experimental observations, all further investigations have been performed with the loading of ~2 nm Ag-NP formulation.

**3.3. High-Speed Nanopatterning Using HIBL.** With significant shreds of evidence on the key role of Ag-NPs in high-resolution patterning by Ter−Ag resist formulation, a high-speed/high-resolution patterning using HIBL was performed and the outcomes were compared with EBL results (Figure 6a,b). A good enhancement in sensitivity of 1 wt % Ter−Ag (~2 nm) was observed; the calculated HIBL sensitivity ($E_{He}$) was 32.12 $\mu$C/cm$^2$ as compared to its EBL sensitivity of ($E_e$) 50−65 $\mu$C/cm$^2$. High-yield 100 and 50 nm L/S HIBL patterns are shown in Figure S14. These patterns exhibited minimum scum formation and small bridging between the developed line patterns. Considering EBL patterns of 12 nm, $L$/10$S$, scum was slightly visible, which may be due to the proximity of the tool, as perceived in Figure 6b. On the other hand, the HIBL-exposed patterns show a solution for proximity issues, as mentioned in Section 1 (results are shown


https://dx.doi.org/10.1021/acsanm.0c01362
ACS Appl. Nano Mater. XXXX, XXX, XXX−XXX

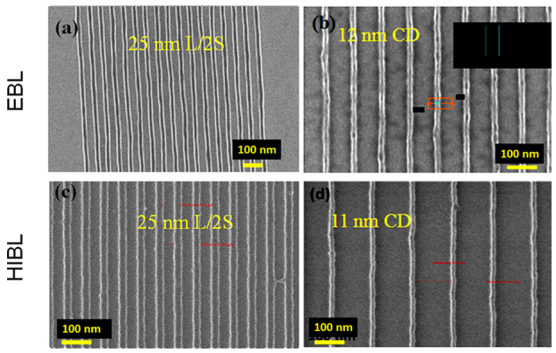


**Figure 6.** High-resolution patterns exposed to e-beam at 50 $\mu C/cm^2$: (a) 25 nm line patterns and (b) 12 nm CD patterns. High-resolution patterns exposed to $He^+$ ion beam at 34.12 $\mu C/cm^2$: (c) 25 nm line patterns and (d) 11 nm CD patterns.

in Figure 6c,d). Defect-free 25 nm $L/2S$ and 11 nm CD line patterns were visualized with negligible scum and line bridging as compared to EBL. This high-resolution study reveals that Ter−Ag can act as a potential HIBL resist with decent sensitivity.

**3.4. Pattern Evaluation through Atomic Force Microscopy.** To establish the robustness of the designed and developed Ter−Ag resist for next-generation technology nodes, the validation of essential processing parameters such as deadhesion, fracturing, and pattern collapse of the Ter−Ag resist was performed through nondestructive, tapping mode mechanical atomic force microscopy (MAFM). Figure 7 shows

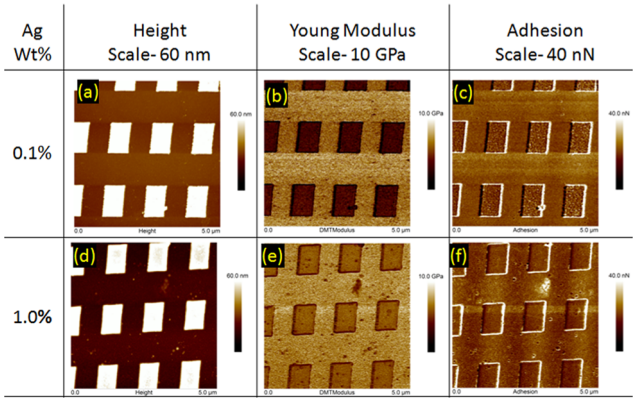


**Figure 7.** AFM analysis of the e-beam-exposed Ter−Ag resist with different wt % values. Dependence of Young's modulus (stiffness) and adhesion of the resist on Ag-NPs' wt %, by observing the height, Young's modulus, and adhesion for 0.1% (a−c) and 1.0% (d−f) resists.

the AFM micrograph of 0.1−1 wt % Ag-NPs in ∼40 nm Ter−Ag resist patterns (see Figure S15). The evolution of adhesion and Young's modulus ($Y$) provides the stiffness of the resist and suggests better etch resistance also. Figure 7a−c depicts the 1 $\mu$m $L/S$ array of 0.1 wt % Ter−Ag; the thickness is recorded as ∼40 nm and the contrast of Young's modulus ($\Delta Y$) between the resist and substrate as ∼2.30 GPa. On the other hand, when 1.0 wt % Ter−Ag were investigated, enhanced stiffness of patterns was observed, $\Delta Y$ of ∼1.1 GPa (Figure 7d−f). The absolute $Y$ values recorded are 4.06 GPa (Figure 7b) and 5.26 GPa (Figure 7e) for 0.1 and 1.0 wt % Ter−Ag resists, respectively, which is much more than the theoretical Young's modulus of Terpolymer (800 MPa). These enhanced values of $Y$ in patterned Ter−Ag could be due to the significant contribution of silicon while measurements. Nevertheless, the comparative study shows the enhancement of $Y$ with increased Ag-NPs.[55,56] It is anticipated that the developed nanoparticle-based hybrid resist may also possess higher etch resistance to the Si-based reactive etchants ($SbF_6^-$).[57]

**3.5. Mechanism for High-Resolution Pattern Formation in the Ter−Ag Resist.** The mechanism for the positive tone formulation of the Terpolymer resist in the presence of PAG is shown in Figure 8a. Upon exposure of the photoacid generator with the ion beam or UV light, a hydrogen ion is released, which further reacts with the ester group present in the Terpolymer. The ester group is converted into carboxylic acid, which is soluble in the developer, thereby forming a positive tone resist. While pristine Terpolymer exposure, an interesting phenomenon is observed that changes the behavior of a common positive tone resist to a negative tone resist. It suggests that the overall polarity change in the Terpolymer matrix (Figure 3a) under high-energy irradiation and the presence of ultrafine Ag-NPs further accelerates this phenomenon.[35] The mechanism for the negative tone formulation of the Ter−Ag resist is shown in Figure 8b. When the Terpolymer was exposed to the irradiation in the absence of PAG, the hydroxyl group present in Terpolymer will undergo dehydration with another moiety and form ether linkage (C−O−C), which is insoluble in the developer, thereby forming a negative tone resist. It is well documented in the literature that the polymer can form different types of radicals when they are exposed to the electron beam.[23] In our current study, the ultrafine Ag-NPs present in the polymer matrix are possibly accelerating the radical formation process through various surface excitation phenomena under irradiation. The polymer radicals formed in the exposed region undergo cross-linking through radical recombination, resulting in various cross-linked structures.[58] Owing to their high molecular weight, the cross-linked products in the exposed area become insoluble in acetonitrile, leading to the formation of a negative tone pattern. Further fundamental studies are planned to undertake the effect of nanoparticles such as Ag-NPs on the dynamics of the electron beam and EUV irradiation of analogous model structures.[59,60]

**3.6. Future Scope: Ter−Ag Resist for Universal Electrode Applications.** With significant incorporation of Ag-NPs in the polymeric resist matrix, it might be possible that the conductivity of the polymer will enhance; the literature also suggests enhancement in conductivity of negative tone resists with Ag.[39,54] Therefore, the developed Ter−Ag resist may also be a potential candidate to directly impose in the nanoelectronic applications, which reduces the process complexity of nanoelectrode fabrication. As a proof-of-concept, a sharp edge four-probe geometry of 100 nm separation with required complex bends is patterned using the 1 wt % Ter−Ag resist formulation, as shown in Figure 9a. The electrical investigation suggests the bilateral $I-V$ characteristic when the current was passed through the Si (100) channel (50 $\mu$m). Figure 9b shows the $I-V$ curves of the resist/Si/resist stacks. Low current conduction in pristine Terpolymer depicts nonconducting behavior majorly due to amorphous hydrocarbons. Meanwhile, the Ter−Ag sample showed enhanced conduction across the channel, which suggests that the Ag-NPs acts as the conduction sites or doping materials for the polymer. The one order improvement in current with 1 wt % Ter−Ag is shown in Figure 9b (red). The intrinsic conductivity/resistivity


https://dx.doi.org/10.1021/acsanm.0c01362
ACS Appl. Nano Mater. XXXX, XXX, XXX−XXX

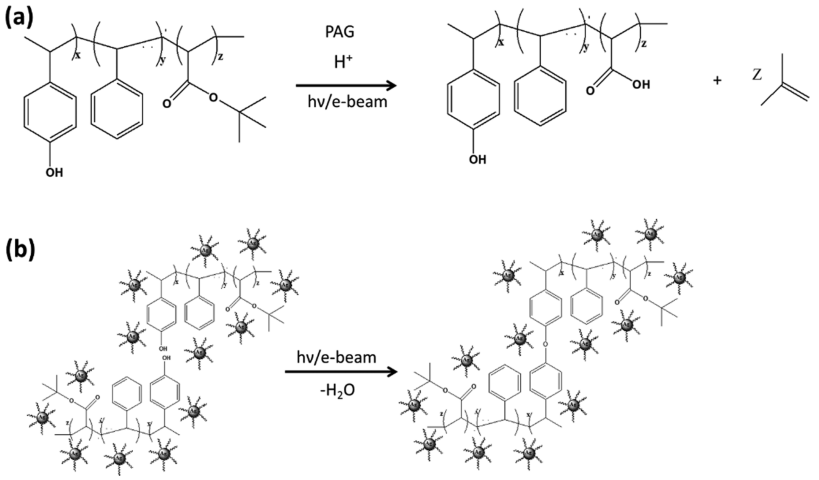


**Figure 8.** Proposed schematic for (a) positive tone patterning of the Ter-Pag resist and (b) negative tone patterning of the Ter−Ag resist through cross-linking.

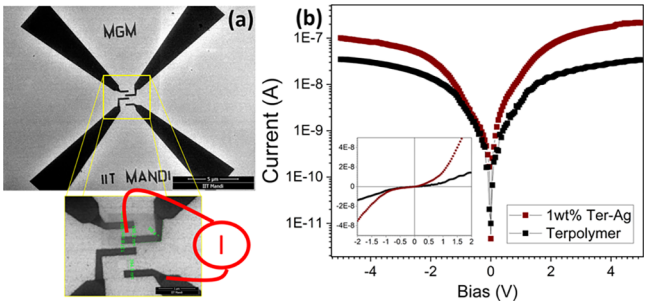


**Figure 9.** Putting Ter−Ag as a contact. SEM micrograph of Ter−Ag patterned as a four-probe contact for direct usage in future electronics. (b) Electrical *I*−*V* investigation of concerned polymer/silicon/polymer structures for Terpolymer and the Ter−Ag material; the *I*−*V* investigation was conducted over the lateral structure were separated with 50 $\mu$m silicon as the substrate; the current values suggested relatively increased conduction.

of the resist formulation was calculated with van der Pauw four-point measurements (detailed experiment schematic is shown in Figure S16, SI-15).[61] The recorded conductivities for pristine Terpolymer and Ter−Ag were found to be $1.18 \times 10^{-2}$ and $5.40 \times 10^{-2}$ S/cm, respectively; these values need further improvement to be used directly and can be done by higher Ag-NPs loading %. This electrical investigation paves the way to directly patternable high-resolution device structures for flexible electronics also.

## 4. CONCLUSIONS

In summary, we report our efforts for addressing the high-resolution/high-sensitivity issue, often associated with many resist formulations, through the development of Ag-NP-embedded polymeric hybrid resists. The blending of different wt % Ag-NPs (0.1−1 wt %) into *tert*-butyl 2-ethyl-6-(4-hydroxyphenyl)-4-phenylheptanoate (Terpolymer) has resulted in various Ter−Ag hybrid resist formulations. The formulated hybrid resists have high sensitivity toward DUV (254 nm) photons, EBL, and HIBL and showed high-resolution patterns also. A decrease in e-beam exposure dose from 600 to 50 $\mu$C/cm$^2$ was optimized by increasing Ag-NP loading inside the resist matrix. We have successfully demonstrated via experimental and simulation evidence that the Ag-NPs act as irradiation sensitizers and enhance the absorption cross section of the resist films. Therefore, the incorporation of high-atomic-number materials (such as Ag) into the polymeric resist network may bring significant improvement in sensitivity, feature size, and LWR/LER, which can be applied in next-generation lithography applications for semiconductor fabrication.

## ■ ASSOCIATED CONTENT

### Supporting Information

The Supporting Information is available free of charge at https://pubs.acs.org/doi/10.1021/acsanm.0c01362.

Synthesis procedure for hydroxystyrene-based Terpolymer (Figure S1); description of the photoacid generator (Figure S2); synthesis of Ag nanoparticles from silver nitrate salt (Figure S3); optical image of the spin-coated thin film of the Ter−Ag resist (Figure S4); particle size determination of synthesized silver nanoparticles by the dynamic light scattering (DLS) method (Figure S5); gel permeation chromatography (GPC) of Terpolymer (Figure S6); DUV study of the Terpolymer resist (Figure S7); DUV study of the Terpolymer−Ag resist (Figure S8); effect of Ag-NP concentration (Figure S9); Monte-Carlo simulations of bare materials as a substrate for stopping power analysis (Figure S10); LER/LWR analysis with Summit software and effect of nanoparticle size on LER/LWR (Figures S11−S13); HIBL of 1 wt % Ter−Ag (Figure S14); electron-resist interaction analysis for the polymeric resist; AFM of the Ter−Ag sample (Figure S15); and resistivity of the spin-coated polymer (Figure S16) (PDF)

## ■ AUTHOR INFORMATION

### Corresponding Authors

**Satinder K. Sharma** − *School of Computing and Electrical Engineering (SCEE), Indian Institute of Technology (IIT)-Mandi, Mandi 175005, Himachal Pradesh, India;* orcid.org/0000-0001-9313-5550; Email: satinder@iitmandi.ac.in

**Kenneth E. Gonsalves** − *School of Basic Sciences (SBS), Indian Institute of Technology (IIT)-Mandi, Mandi 175005, Himachal Pradesh, India*; Email: kenneth@iitmandi.ac.in



https://dx.doi.org/10.1021/acsanm.0c01362
ACS Appl. Nano Mater. XXXX, XXX, XXX−XXX

### Authors

**Mohamad G. Moinuddin** − *School of Computing and Electrical Engineering (SCEE), Indian Institute of Technology (IIT)-Mandi, Mandi 175005, Himachal Pradesh, India*

**Rudra Kumar** − *School of Computing and Electrical Engineering (SCEE), Indian Institute of Technology (IIT)-Mandi, Mandi 175005, Himachal Pradesh, India;* orcid.org/0000-0002-6190-7779

**Midathala Yogesh** − *School of Basic Sciences (SBS), Indian Institute of Technology (IIT)-Mandi, Mandi 175005, Himachal Pradesh, India*

**Shivani Sharma** − *School of Computing and Electrical Engineering (SCEE), Indian Institute of Technology (IIT)-Mandi, Mandi 175005, Himachal Pradesh, India;* orcid.org/0000-0002-3247-7327

**Manoj Sahani** − *School of Computing and Electrical Engineering (SCEE), Indian Institute of Technology (IIT)-Mandi, Mandi 175005, Himachal Pradesh, India*

Complete contact information is available at: https://pubs.acs.org/10.1021/acsanm.0c01362


### Notes

The authors declare no competing financial interest.

## ■ ACKNOWLEDGMENTS


The authors thank the Department of Science and Technology (DST) and Technology Systems Development Program (TSDP), India for financial support (sanctioned project reference number DST/TSG/AMT/2015/634). R.K. thanks the Science and Engineering Research Board (SERB), New Delhi, India for the national postdoc fellowship (sanction project reference number PDF/2017/001437). M.G.M. thanks the Ministry of Electronics & Information Technology for a research fellowship under the Visvesvaraya Ph.D. Scheme. M.Y. thanks the Council of Scientific and Industrial Research (CSIR), New Delhi, India for a senior research fellowship. The authors acknowledge the Centre for Design and Fabrication of Electronic Devices (C4DFED) and class 100 cleanroom facility of the Indian Institute of Technology (IIT) Mandi, India for various sample preparation facilities and state-of-the-art EBL patterning facilities for the lithography work. The authors thank Advance Material Research Center (AMRC), Indian Institute of Technology (IIT) Mandi, India, for material characterizations. The authors thank Dr. Subrato Ghosh, IIT Mandi for guidance and discussion in Terpolymer synthesis and manuscript drafting. S.S. and M.G.M. acknowledge the contribution of Dr. Rohit Sharma, JUIT, Waknaghat for Ag-NP synthesis; Dr. Jerome Peter, IIT Mandi for Ter-PAG analysis; and Kumar Palit, IIT Mandi for AFM investigation during COVID-19 pendamic. The authors are also thankful to HIM Center, Carl Zeiss Microscopy, Peabody, USA for HIBL exposure and their constant technical support.


## ■ REFERENCES


(1) Jonkers, J. High Power Extreme Ultra-Violet (EUV) Light Sources for Future Lithography. *Plasma Sources Sci. Technol.* **2006**, *15*, S8−S16.

(2) Li, L.; Liu, X.; Pal, S.; Wang, S.; Ober, C. K.; Giannelis, E. P. Extreme Ultraviolet Resist Materials for Sub-7 nm Patterning. *Chem. Soc. Rev.* **2017**, *46*, 4855−4866.

(3) Buitrago, E.; Kulmala, T. S.; Fallica, R.; Ekinci, Y. Chapter 4—EUV Lithography Process Challenges. *Front. Nanosci.* **2016**, *11*, 135−176.

(4) Wu, B.; Kumar, A. Extreme Ultraviolet Lithography: A Review. *J. Vac. Sci. Technol., B* **2007**, *25*, 1743−1761.

(5) Kemp, K.; Wurm, S. EUV Lithography. *C. R. Phys.* **2006**, *7*, 875−886.

(6) Banine, V.; Moors, R. Plasma Sources for EUV Lithography Exposure Tools. *J. Phys. D: Appl. Phys.* **2004**, *37*, 3207−3212.

(7) Furukawa, T.; Naruoka, T.; Nakagawa, H.; Miyata, H.; Shiratani, M.; Hori, M.; Dei, S.; Ayothi, R.; Hishiro, Y.; Nagai, T. In *Novel EUV Photoresist for Sub-7 nm Node*, Society of Photo-Optical Instrumentation Engineers (SPIE) Conference Series; 2017; p 101430X.

(8) Nagai, T.; Nakagawa, H.; Naruoka, T.; Dei, S.; Tagawa, S.; Oshima, A.; Nagahara, S.; Shiraishi, G.; Yoshihara, K.; Terashita, Y.; Minekawa, Y.; Buitrago, E.; Ekinci, Y.; Yildirim, O.; Meeuwissen, M.; Hoefnagels, R.; Rispens, G.; Verspaget, C.; Maas, R. Novel High Sensitivity EUV Photoresist for Sub-7 nm Node. *J. Photopolym. Sci. Technol.* **2016**, *29*, 475−478.

(9) Brown, G. D.; Watkins, J. J. Materials Issues and Modeling for Device Nanofabrication. *Mater. Res. Soc. Symp. Proc.* **1999**, *584*, No. 169.

(10) Shi, X.; Prewett, P.; Huq, E.; Bagnall, D. M.; Robinson, A. P. G.; Boden, S. A. Helium Ion Beam Lithography on Fullerene Molecular Resists for Sub-10nm Patterning. *Microelectron. Eng.* **2016**, *155*, 74−78.

(11) Li, W.-D.; Wu, W.; Williams, R. S. Combined Helium Ion Beam and Nanoimprint Lithography Attains 4-nm Half-Pitch Dense Patterns. *J. Vac. Sci. Technol., B* **2012**, *30*, No. 06F304.

(12) Baek, I.-B.; Yang, J.-H.; Cho, W.-J.; Ahn, C.-G.; Im, K.; Lee, S. Electron Beam Lithography Patterning of Sub-10nm Line Using Hydrogen Silsesquioxane for Nanoscale Device Applications. *J. Vac. Sci. Technol., B* **2005**, *23*, 3120−3123.

(13) Chang, T. H. P.; Mankos, M.; Lee, K. Y.; Muray, L. P. Multiple Electron-Beam Lithography. *Microelectron. Eng.* **2001**, *57−58*, 117−135.

(14) Sidorkin, V.; van Veldhoven, E.; van der Drift, E.; Alkemade, P.; Salemink, H.; Maas, D. Sub-10-Nm Nanolithography with a Scanning Helium Beam. *J. Vac. Sci. Technol., B* **2009**, *27*, L18−L20.

(15) Flatabø, R.; Agarwal, A.; Hobbs, R.; Greve, M. M.; Holst, B.; Berggren, K. K. Exploring Proximity Effects and Large Depth of Field in Helium Ion Beam Lithography: Large-Area Dense Patterns and Tilted Surface Exposure. *Nanotechnology* **2018**, *29*, No. 275301.

(16) Lewis, S. M.; Hunt, M. S.; DeRose, G. A.; Alty, H. R.; Li, J.; Wertheim, A.; De Rose, L.; Timco, G. A.; Scherer, A.; Yeates, S. G.; Winpenny, R. E. P. Plasma-Etched Pattern Transfer of Sub-10 nm Structures Using a Metal-Organic Resist and Helium Ion Beam Lithography. *Nano Lett.* **2019**, *19*, 6043−6048.

(17) Maas, D.; van Veldhoven, E.; van Langen-Suurling, A.; Alkemade, P. F. A.; Wuister, S.; Hoefnagels, R.; Verspaget, C.; Meessen, J.; Fliervoet, T. In *Evaluation of EUV Resist Performance Below 20 nm Cd Using Helium Ion Lithography*, SPIE Proceedings; 2014; Vol. *9048*.

(18) Gallatin, G.; Naulleau, P.; Brainard, R. In *Fundamental Limits to EUV Photoresist*, SPIE Proceedings; 2007; Vol. *6519*.

(19) Grigorescu, A. E.; Hagen, C. W. Resists for Sub-20-nm Electron Beam Lithography with a Focus on Hsq: State of the Art. *Nanotechnology* **2009**, *20*, No. 292001.

(20) Brock, D. C. Patterning the World: The Rise of Chemically Amplified Photoresists | Science History Institute. https://www.sciencehistory.org/distillations/patterning-the-world-the-rise-of-chemically-amplified-photoresists. (accessed August 2, 2020).

(21) Nandi, S.; Yogesh, M.; Reddy, P. G.; Sharma, S. K.; Pradeep, C. P.; Ghosh, S.; Gonsalves, K. E. A Photoacid Generator Integrated Terpolymer for Electron Beam Lithography Applications: Sensitive Resist with Pattern Transfer Potential. *Mater. Chem. Front.* **2017**, *1*, 1895−1899.

(22) Peter, J.; Moinuddin, M. G.; Ghosh, S.; Sharma, S. K.; Gonsalves, K. E. Organotin in Nonchemically Amplified Polymeric Hybrid Resist Imparts Better Resolution with Sensitivity for Next-Generation Lithography. *ACS Appl. Polym. Mater.* **2020**, *2*, 1790−1799.




https://dx.doi.org/10.1021/acsanm.0c01362
ACS Appl. Nano Mater. XXXX, XXX, XXX−XXX

(23) Gangnaik, A. S.; Georgiev, Y. M.; Holmes, J. D. New Generation Electron Beam Resists: A Review. *Chem. Mater.* **2017**, *29*, 1898−1917.
(24) Hu, Y.; Wu, H.; Gonsalves, K.; Merhari, L. Nanocomposite Resists for Electron Beam Nanolithography. *Microelectron. Eng.* **2001**, *56*, 289−294.
(25) Gonsalves, K. E.; Merhari, L.; Wu, H.; Hu, Y. Organic-Inorganic Nanocomposites: Unique Resists for Nanolithography. *Adv. Mater.* **2001**, *13*, 703−714.
(26) Ghosh, S.; Pradeep, C. P.; Sharma, S. K.; Reddy, P. G.; Pal, S. P.; Gonsalves, K. E. Recent Advances in Non-Chemically Amplified Photoresists for Next Generation IC Technology. *RSC Adv.* **2016**, *6*, 74462−74481.
(27) Reddy, P. G.; Pal, S. P.; Kumar, P.; Pradeep, C. P.; Ghosh, S.; Sharma, S. K.; Gonsalves, K. E. Polyarylenesulfonium Salt as a Novel and Versatile Nonchemically Amplified Negative Tone Photoresist for High-Resolution Extreme Ultraviolet Lithography Applications. *ACS Appl. Mater. Interfaces* **2017**, *9*, 17−21.
(28) Kosma, V.; De Simone, D.; Vandenberghe, G. Metal Based Materials for EUV Lithography. *J. Photopolym. Sci. Technol.* **2019**, *32*, 179−183.
(29) Santillan, J.; Itani, T. Characterization Studies on Metal-Based EUV Resist Film Properties. *J. Photopolym. Sci. Technol.* **2018**, *31*, 663−667.
(30) Kumar, R.; Chauhan, M.; Moinuddin, M. G.; Sharma, S. K.; Gonsalves, K. E. Development of Nickel-Based Negative Tone Metal Oxide Cluster Resists for Sub-10 nm Electron Beam and Helium Ion Beam Lithography. *ACS Appl. Mater. Interfaces* **2020**, *12*, 19616−19624.
(31) Sharma, S.; Kumar, R.; Chauhan, M.; Moinuddin, M.; Peter, J.; Ghosh, S.; Pradeep, C.; Gonsalves, K. *All-New Nickel-Based Metal Core Organic Cluster (MCOC) Resist for N7 + Node Patterning*, SPIE Proceedings; 2020; Vol. *11326*.
(32) Kozawa, T.; Tagawa, S. Radiation Chemistry in Chemically Amplified Resists. *Jpn. J. Appl. Phys.* **2010**, *49*, No. 030001.
(33) Reichmanis, E.; Houlihan, F. M.; Nalamasu, O.; Neenan, T. X. Chemical Amplification Mechanisms for Microlithography. *Chem. Mater.* **1991**, *3*, 394−407.
(34) Brown, A.; Arnold, W. In *Optimization of Resist Optical Density for High Resolution Lithography on Reflective Surfaces*, SPIE Proceedings, 1985; Vol. *0539*.
(35) Jeyakumar, A.; Henderson, C. In *A Comparative Study between Organic and Inorganic Resists in Electron Beam Lithography Using Monte Carlo Simulations*, SPIE Proceedings; 2003; Vol. *5039*.
(36) Cardineau, B.; Robinson, A.; Lawson, R. Chapter 11−Molecular Organometallic Resists for EUV (MORE). *Front. Nanosci.* **2016**, *11*, 377−420.
(37) Fallica, R.; Haitjema, J.; Wu, L.; Castellanos Ortega, S.; Brouwer, A.; Ekinci, Y. Absorption Coefficient of Metal-Containing Photoresists in the Extreme Ultraviolet. *J. Micro/Nanolithogr., MEMS, MOEMS* **2018**, *17*, No. 023505.
(38) De Simone, D.; Sayan, S.; Dei, S.; Pollentier, I.; Kuwahara, Y.; Vandenberghe, G.; Nafus, K.; Shiratani, M.; Nakagawa, H.; Naruoka, T. In *Novel Metal Containing Resists for EUV Lithography Extendibility*, SPIE Proceedings; 2016; Vol. *9776*.
(39) Bhuvana, T.; Subramaniam, C.; Pradeep, T.; Kulkarni, G. U. Conducting Nanocrystal Patterns Using a Silver Organic Complex Blended with Polystyrene as E-Beam Resist. *J. Phys. Chem. C* **2009**, *113*, 7038−7043.
(40) Lee, S. W.; Zamani, H.; Feng, P. X.-L.; Sankaran, R. M. Extraction of a Low-Current Discharge from a Microplasma for Nanoscale Patterning Applications at Atmospheric Pressure. *J. Vac. Sci. Technol., B* **2012**, *30*, No. 010603.
(41) Gerardo, C. D.; Cretu, E.; Rohling, R. Fabrication of Circuits on Flexible Substrates Using Conductive SU-8 for Sensing Applications. *Sensors* **2017**, *17*, No. 1420.
(42) Marques-Hueso, J.; Morton, J. A. S.; Wang, X.; Bertran-Serra, E.; Desmulliez, M. P. Y. Photolithographic Nanoseeding Method for Selective Synthesis of Metal-Catalysed Nanostructures. *Nanotechnology* **2018**, *30*, No. 015302.
(43) Kim, S.; Kim, B.; Cho, S. M.; Lee, H.-J.; Hwang, B. Etchant-Free Patterning of Silver Nanowire Transparent Electrode Using Dry-Film Photoresists for Organic Light-Emitting Diodes. *Mater. Lett.* **2017**, *209*, 433−436.
(44) Kim, S.; Hwang, B. Ag Nanowire Electrode with Patterned Dry Film Photoresist Insulator for Flexible Organic Light-Emitting Diode with Various Designs. *Mater. Des.* **2018**, *160*, 572−577.
(45) Yamachika, M.; Kobayashi, E.; Ota, T. Radiation Sensitive Resin Composition. U.S. Patent US5,679,4951994.
(46) Cutler, C.; Thackeray, J.; DeSisto, J.; Nelson, J.; Lee, C.-B.; Li, M.; Aqad, E.; Hou, X.; Marangoni, T.; Kaitz, J.; Rena, R.; Mack, C. In *Roughness Power Spectral Density as a Function of Resist Parameters and Its Impact through Process*, SPIE Proceedings; 2018; Vol. *10587*.
(47) Demers, H.; Poirier-Demers, N.; Couture, A. R.; Joly, D.; Guilmain, M.; de Jonge, N.; Drouin, D. Three-Dimensional Electron Microscopy Simulation with the Casino Monte Carlo Software. *Scanning* **2011**, *33*, 135−146.
(48) Koleva, E.; Vutova, K.; Asparuhova, B.; Kostic, I.; Cvetkov, K.; Gerasimov, V. Modeling Approaches for Electron Beam Lithography. *J. Phys.: Conf. Ser.* **2018**, *1089*, No. 012016.
(49) Greve, M. M.; Holst, B. Optimization of an Electron Beam Lithography Instrument for Fast, Large Area Writing at 10-KV Acceleration Voltage. *J. Vac. Sci. Technol., B* **2013**, *31*, No. 043202.
(50) Barclay, G. G.; Cronin, M. F.; DellaGuardia, R. A.; Thackeray, J. W.; Ito, H.; Breyta, G. Novel Copolymers and Photoresist Compositions Comprising Copolymer Resin Binder Component. EU Patent EP1669803B12000.
(51) Cui, Z. *Nanofabrication Principles, Capabilities and Limits*, 2nd ed.; Springer International Publishing, 2017.
(52) Weyland, M.; Midgley, P. A.; Thomas, J. M. Electron Tomography of Nanoparticle Catalysts on Porous Supports: A New Technique Based on Rutherford Scattering. *J. Phys. Chem. B* **2001**, *105*, 7882−7886.
(53) Pollentier, I.; Vesters, Y.; Jiang, J.; Vanelderen, P.; de Simone, D. In *Unraveling the Role of Secondary Electrons Upon Their Interaction with Photoresist During EUV Exposure*, SPIE Proceedings; 2017; Vol. *10450*.
(54) Jiguet, S.; Bertsch, A.; Hofmann, H.; Renaud, P. In *Conductive SU8-Silver Composite Photopolymer*, 17th IEEE International Conference on Micro Electro Mechanical Systems. Maastricht MEMS 2004 Technical Digest; 2004; pp 125−128.
(55) Lu, S. G.; Chen, X.; Levard, T.; Diglio, P. J.; Gorny, L. J.; Rahn, C. D.; Zhang, Q. M. Large Displacement in Relaxor Ferroelectric Terpolymer Blend Derived Actuators Using Al Electrode for Braille Displays. *Sci. Rep.* **2015**, *5*, No. 11361.
(56) Sharma, S. K.; Pal, S. P.; Reddy, P. G.; Kumar, P.; Ghosh, S.; Gonsalves, K. E. Design and Development of Low Activation Energy Based Nonchemically Amplified Resists (N-Cars) for Next Generation EUV Lithography. *Microelectron. Eng.* **2016**, *164*, 115−122.
(57) Huang, Z. P.; Geyer, N.; Werner, P.; de Boor, J.; Gosele, U. Metal-Assisted Chemical Etching of Silicon: A Review. *Adv. Mater.* **2011**, *23*, 285−308.
(58) Park, S.; Yoo, S. H.; Kang, H. R.; Jo, S. M.; Joh, H.-I.; Lee, S. Comprehensive Stabilization Mechanism of Electron-Beam Irradiated Polyacrylonitrile Fibers to Shorten the Conventional Thermal Treatment. *Sci. Rep.* **2016**, *6*, No. 27330.
(59) Satyanarayana, V. S. V.; Kessler, F.; Singh, V.; Scheffer, F. R.; Weibel, D. E.; Ghosh, S.; Gonsalves, K. E. Radiation-Sensitive Novel Polymeric Resist Materials: Iterative Synthesis and Their EUV Fragmentation Studies. *ACS Appl. Mater. Interfaces* **2014**, *6*, 4223−4232.
(60) Singh, V.; Satyanarayana, V. S. V.; Batina, N.; Reyes, I. M.; Sharma, S.; Kessler, F.; Scheffer, F.; Weibel, D.; Ghosh, S.; Gonsalves, K. Performance Evaluation of Nonchemically Amplified Negative Tone Photoresists for E-Beam and EUV Lithography. *J. Micro/Nanolithogr., MEMS, MOEMS* **2014**, *13*, No. 043002.


https://dx.doi.org/10.1021/acsanm.0c01362
*ACS Appl. Nano Mater.* XXXX, XXX, XXX−XXX

(61) Keithley. van der Pauw and Hall Voltage Measurements with the 4200A-SCS Parameter Analyzer | Tektronix. https://in.tek.com/document/application-note/van-der-pauw-and-hall-voltage-measurements-4200a-scs-parameter-analyzer (accessed August 02, 2020).



https://dx.doi.org/10.1021/acsanm.0c01362
ACS Appl. Nano Mater. XXXX, XXX, XXX−XXX